International Journal of Refractory Metals and Hard Materials 101 (2021) 105657

Contents lists available at ScienceDirect

International Journal of Refractory Metals and Hard Materials

journal homepage: www.elsevier.com/locate/IJRMHM

The effect of ball to powder ratio on the processing of a novel Mo-Cu-Al_2O_3 composite

Dániel Pethő [a,*], Tamás Kurusta [b], Ferenc Kristály [c], Tamás Mikó [a], Zoltán Gácsi [a]

[a] Institute of Physical Metallurgy, Metalforming and Nanotechnology, University of Miskolc, Hungary
[b] Institute of Raw Material Preparation and Environmental Processing, University of Miskolc, Hungary
[c] Institute of Mineralogy and Geology, University of Miskolc, Hungary

ARTICLE INFO

Keywords:
Milling
Pseudo-alloy
Metal matrix composite
Hot pressing
Recrystallization

ABSTRACT

In the present article a 45Mo-45Cu-10Al_2O_3 (wt%) nano-composite was produced by mechanical alloying, shaped by cold pressing then by hot pressing at 950 °C. Our aim was to investigate the effect of different ball to powder ratio (BPR) on the particle size and shape, as well as on the material composition. Investigations were done with XRD, SEM and for hot pressed specimens Brinell hardness measurement. Lower BPR resulted in nano-sized crystallites in the powder, a homogenous phase distribution and higher BPR resulted in even smaller crystallite sizes, but with ZrO_2 contamination from the milling equipment. The milling resulted in two separate fractions in the metallic phases separated by crystallite size, strain and lattice parameter. After hot pressing, the lower BPR powders developed a homogeneous, evenly distributed microstructure. Cu recrystallized during hot pressing, but still remained nanocrystalline, the crystallite size of Mo and α-Al_2O_3 decreased even more due to crystallite deformation and in the case of Mo, the lattice strain values indicates that recovery had also happened. The heating eliminated the crystal defects at highly strained areas and the subsequent cooling evened out the stresses in the respective metallic phases. The inner grain structure was revealed by etching, showing that α-Al_2O_3 particles congregated only at the Mo grain boundaries, but penetrated the Cu grains. The lattice strain values combined with the BSE images reveal that the Cu is the main matrix of the α-Al_2O_3 particles. The results indicate that the α-Al_2O_3 particles induced Particle Stimulated Nucleation (PSN) in the Cu explaining its moderate crystallite size increase. The hot pressed samples of higher BPR had higher ceramic (ZrO_2 and α-Al_2O_3) content, resulting in higher hardness, but lower relative density (92.4%), compared to the samples of lower BPR, which reached 97.2% relative density and hardness still significantly higher than Mo—Cu alloys.

1. Introduction

Thermal management materials are used in fundamental parts of microelectronics packaging. Their main goal is to dissipate the generated heat to the ambient environment, and to provide the necessary structural integrity (hardness, strength) [1–3], this applies especially in the case of larger parts such as PCB heat sinks [4]. Generally, Mo—Cu and W—Cu pseudo-alloys are used for heat dissipation due to their high temperature applicability. The copper provides excellent heat conductivity, and the refractory metals provide high temperature strength. Mo—Cu is more advantageous than W—Cu, given its lower density and good formability above 30% Cu content. Since Mo and Cu are immiscible in each other, mechanical alloying is used to produce the raw composites, which also makes the product homogenous, nanocrystalline and having high hardness [5,6]. To preserve the nanostructure, during the hot pressing/sintering process, it is beneficial to stay below the melting temperature of Cu, [7–9]. Nevertheless temperature above the Cu melting point is also applied, in these cases the optimal processing temperature is ranging between 1100 and 1150 °C [10–14].

Ceramic reinforcement is often introduced to improve the mechanical properties of metals, creating metal matrix composites (MMCs) [15–20]. Al_2O_3 is a known ceramic material for strengthening Mo and Cu separately [21–27], but the addition of Al_2O_3 to Mo—Cu pseudo alloys is a seldom researched topic. The benefit of Al_2O_3 is that it has a low coefficient of thermal expansion (CTE) so it reduces the CTE of composite. Its high hardness improves mechanical resistance, moreover its low density (3.98 g/cm^3) is beneficial in weight sensitive areas [2].

* Corresponding author.
E-mail address: femdani@uni-miskolc.hu (D. Pethő).

https://doi.org/10.1016/j.ijrmhm.2021.105657
Received 25 May 2021; Received in revised form 12 July 2021; Accepted 26 July 2021
Available online 31 July 2021

Previous studies of Mo-Cu-Al_2O_3 focused mainly on the feasibility of mechanochemical production, not on the characterization of the bulk product [28,29]. Other studies focused on creating an Al_2O_3-Mo-Cu composite with an Al_2O_3 content of 85 vol% which mainly focused on improving the crack resistance of the alumina [30,31].

The aim of this work is to investigate the effect of changing BPR on the characteristics of the Mo-Cu-Al_2O_3 nano-composite both in powder and in hot pressed bulk state.

2. Material and methods

The composite powders with the composition of 45Mo-45Cu-10Al_2O_3 (wt%) were milled with Fritsch Pulverisette 5 planetary ball mill. The used Mo, Cu and α-Al_2O_3 powders were Alfa Aesar 10,030, 42,689 and 42,572, respectively. Ar gas atmosphere was used to prevent oxidation, 1 wt% ethanol was added as a process controlling agent (PCA) [6,32], so the powder would not adhere to the milling equipment and to control excessive cold welding. After preliminary tests, 400 rpm was found optimal. The milling jar and balls (20 mm Ø) are of ZrO_2, thus evading the problem of Fe contamination caused by steel milling equipment. Minimal mill abrasion and the desired nanocrystalline state was possible to produce with two different BPR: 2.5 BPR and 5 BPR. In this article the milled powders and the pressed bulk specimens are coded accordingly.

The milled powders were cold pressed with 1.5 GPa to obtain cylindrical green specimens (3 parallel specimens from each powder) using the Instron 5900. Before and during the process the equipment was placed under vacuum with 10^{-3} mbar to remove the residual air from between the particles, so it would not oxidize them during hot pressing. Graphite spray was used as lubricant. After cold pressing the samples were hot pressed uniaxially at 950 °C with 150 MPa, 190 °C/min heating rate and 10 min holding time, using the Eurotherm 2208e for temperature control and the Iew5 induction heating unit with the power of 2 kW. During the process Al_2O_3 powder was used as both sealant and medium for pressure transmission. The experimental production route can be seen on Fig. 1.

The density of the cylindrical samples (8.35 ± 0.05 mm in diameter and 6.1 ± 0.3 mm in height) were measured using Archimedes method. Afterwards, the cylindrical samples were cut in half perpendicularly to their axis. The XRD measurements regarding crystallite size, lattice parameter and strain, were carried out with Bruker D8 Discover (Cu K-alpha 1,2 radiation, 40 kV and 40 mA generator settings, Bragg-Brentano geometry, LynxEye XE-T energy dispersive position sensitive detector in 1D mode, counting time 0.007°(2Th)/124 s) on the inner sectioned surface. Rietveld refinement was applied in TOPAS4 for evaluation of the results, calibrated with a corundum standard (NIST SRM 1976) and Fundamental Parameters Approach (FPA) was adopted for the instrumental profile [33]. The Inorganic Crystal Structure Database (ICSD) was used to retrieve the crystal structure data. The peak broadening was resolved by simultaneous size and strain calculation [size: $d_{cry} = FWHM(2\theta)*\cos(\theta)/\lambda$; strain: $\varepsilon_0 = FWHM(2\theta)/(4\tan\theta)$]. The March-Dollase function was used to resolve for preferred orientation where needed [34]. In the case of the milled powders the modeling could not be solved with a single structure of each phase, therefore a second structure was introduced for each metallic phase [35] differing in unit cell parameters, crystallite size and strain, fitted against the measured pattern. The outlined workflow of the analysis can be seen on Fig. 2. Fitting of atomic coordinates and thermal parameters was not required, presence of amorphous phases was not observed.

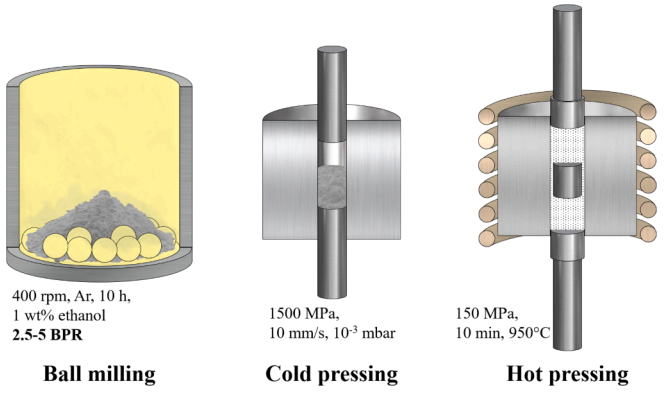

Fig. 1. The manufacturing steps in order from left to right: ball milling, cold pressing and hot pressing.

The other half of the sectioned samples were grinded and polished to a 0.3 μm surface finish for SEM examination with Helios G4 PFIB-SEM (ABS detector, 20 kV, 1.6 nA current). The etching of the samples were carried out on the polished surfaces with 10 s immersion time for Mo and 15 s immersion time for Cu. Subsequent to immersion, the samples were cleaned with distilled water and then with ethanol before drying. The solvent for Mo was Murakami's reagent (ASTM 98C) consisting of 10 g $K_3Fe(CN)_6$, 10 g NaOH and 100 mL distilled H_2O. The solvent for Cu contained 1 g $K_2Cr_2O_7$, 4 mL H_2SO_4 and 50 mL distilled H_2O (simply referred to as potassium dichromate). The microstructure of the selectively etched samples were also examined by SEM. The hardness measurements were carried out with Wolpert UH 930 with HB 2.5/62.5 on all the three parallel samples of 2.5 BPR and 5 BPR.

3. Results and discussion

3.1. Powders

After milling the dried and homogenized powders were analyzed by XRD. Differences of the milled powders with different BPR can be seen on diffractograms in Fig. 3 a). The 2.5 BPR pattern displays sharp and high peaks. Compared to 2.5 BPR, the peaks on the 5 BPR pattern are broadened and lost height, indicating that the more intensive milling decreased crystallite sizes and generated lattice strain. The peaks of ZrO_2 (baddeleyite) from the milling equipment are also present, as contamination. This can be explained by the fact that increasing BPR reduces the mean free path of the milling ball's motion, so it increases impact frequency, but it also increases contamination [5]. Therefore the increased BPR clearly leads to more significant decrease in crystallite sizes. Based on the fact that the maximum values of the Mo and Cu peaks did not change due to the milling and the peaks remain symmetrical, neither Mo (Cu) or Cu(Mo) solid solutions have been formed in either sample, since their development requires considerably longer milling time [36]. After milling, the 2.5 BPR sample had nominal composition with 1 wt% Cu_2O. The 5 BPR sample was contaminated with 9 wt% ZrO_2 due to the higher ball to powder ratio [5,37]. The amount of Cu_2O was found to be 3 wt%, explained by sample inhomogeneity and the minimal adherence of Mo and Cu to the milling equipment, since the oxide content of Cu powder was 2 wt%. The detailed analysis of the 2.5 BPR milled powder with separate diffractograms plotted for each phase can be seen on Fig. 2b). The difference curve is shown as the indicator of the goodness of the fitting. As it can be seen the metallic phases in both samples had two distinct fractions. These are identified by the distinct crystallite size ranges (higher and lower), as shown in Table 1. The size ranges are associated with different lattice strain values (Fig. 6), reflected by the unit cell parameters also. The lattice strain reflects all distortions in the crystal structure, including lattice defects, vacancies, and dislocations [38,39]. Dislocation density increases by milling [5,6,32] leading to size and strain delimited phase fractions, which in our experiments are parameters more significantly describing material evaluation, than dislocation density variations. These differences can be seen on the diffractograms as their respective peaks have different height and broadening (FWHM). The reason behind the formation of distinct size fractions is different for Mo and Cu. The Mo particles either weld together during milling, forming a larger particle, or get flattened by the

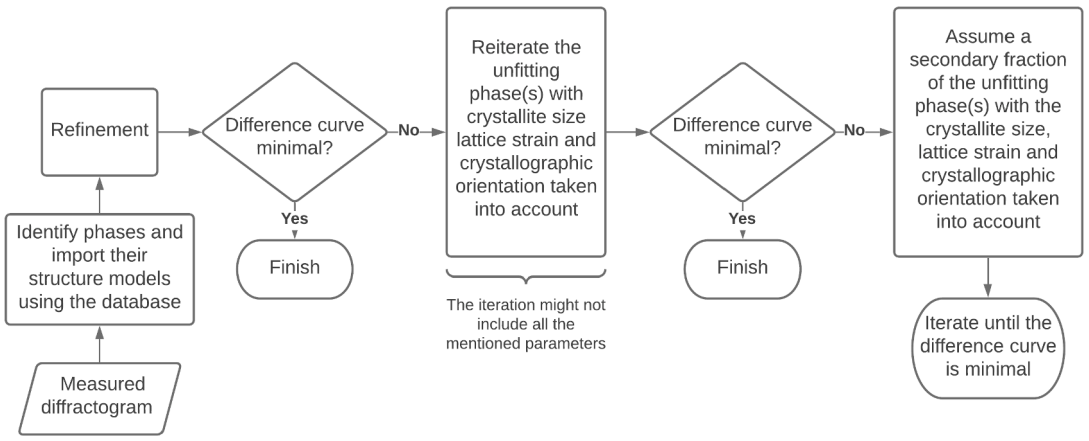

Fig. 2. The flowchart of the Rietveld analysis.

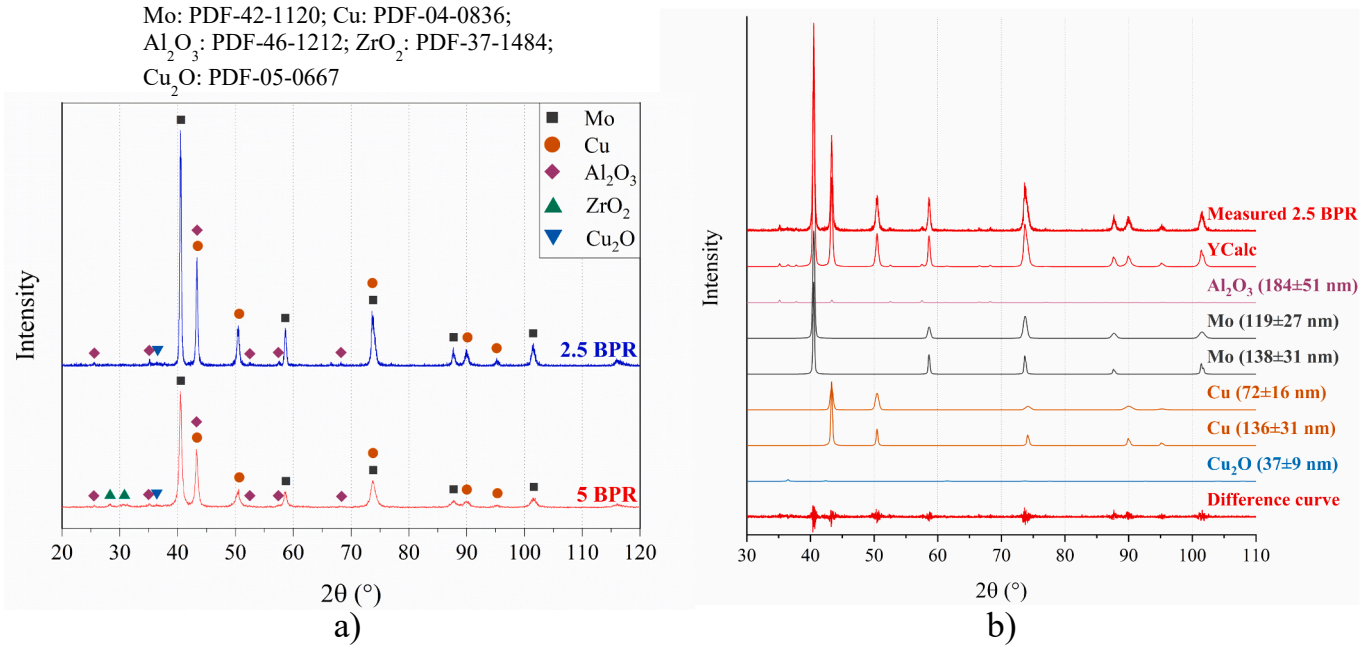

Fig. 3. The X-ray diffractograms of the milled powders. a) the comparison of the milled powders; b) the analysis of the 2.5 BPR powder shown in detailed view.

Table 1
The average crystallite size and weight percentage of the phases in the base and milled powders.

	Mo		Cu		α-Al_2O_3		ZrO_2
	nm/wt%		nm/wt%		nm/wt%		nm/wt%
	Coarser	Finer	Coarser	Finer	Coarser	Finer	
Base powders	4090 ± 910/100 wt%		465 ± 103/58.9 wt%	108 ± 24/38.7 wt%	783 ± 217/17.1 wt%	146 ± 40/82.9 wt%	
2.5 BPR	138 ± 31/25.7 wt%	119 ± 27/19.9 wt%	136 ± 30/19.4 wt%	72 ± 16/24.5 wt%	184 ± 51/9.5 wt%		
5 BPR	156 ± 35/10.8 wt%	16 ± 4/29.7 wt%	56 ± 12/7.0 wt%	16 ± 3/30 wt%	114 ± 32/10.8 wt%		10 ± 2/8.9 wt%

milling balls, therefore the deformation and the resulting lattice strain is higher (Fig. 8a). Cu particles can also weld together (with low α-Al_2O_3 content), or form a mixture with α-Al_2O_3 (Fig. 8 a and b) where the ceramic particles induce dislocations in their vicinity resulting in higher distortion of the Cu lattice [40]. The base Cu powder also had two fractions, but it had no effect on the formation of two distinct size fractions in the milled powders. The single size fraction of the α-Al_2O_3 compared to the base powder is due to the higher abrasion of the larger particles during milling. It can be seen in Table 1 that 2.5 BPR had its constituents between 100 and 190 nm, while the phases in 5 BPR are smaller due to the higher BPR [6]. The ZrO_2 crystallites originating from the mill are 10 nm in size, corundum is around 100 nm. In both milled powders the crystallite sizes are considerably lower than in the base powders and in most phases the finer fraction has higher weight percentage than the coarse fraction.

The SEM back-scattered electron images of the powders are shown on Fig. 4. The particles in the 2.5 BPR sample are sharp-edged, flattened, the phase distribution is homogenous, but the phases are separated, and are easily distinguished due to the differences in average atomic numbers (Mo bright, Cu dark, α-Al_2O_3 black dots). In 5 BPR the particles

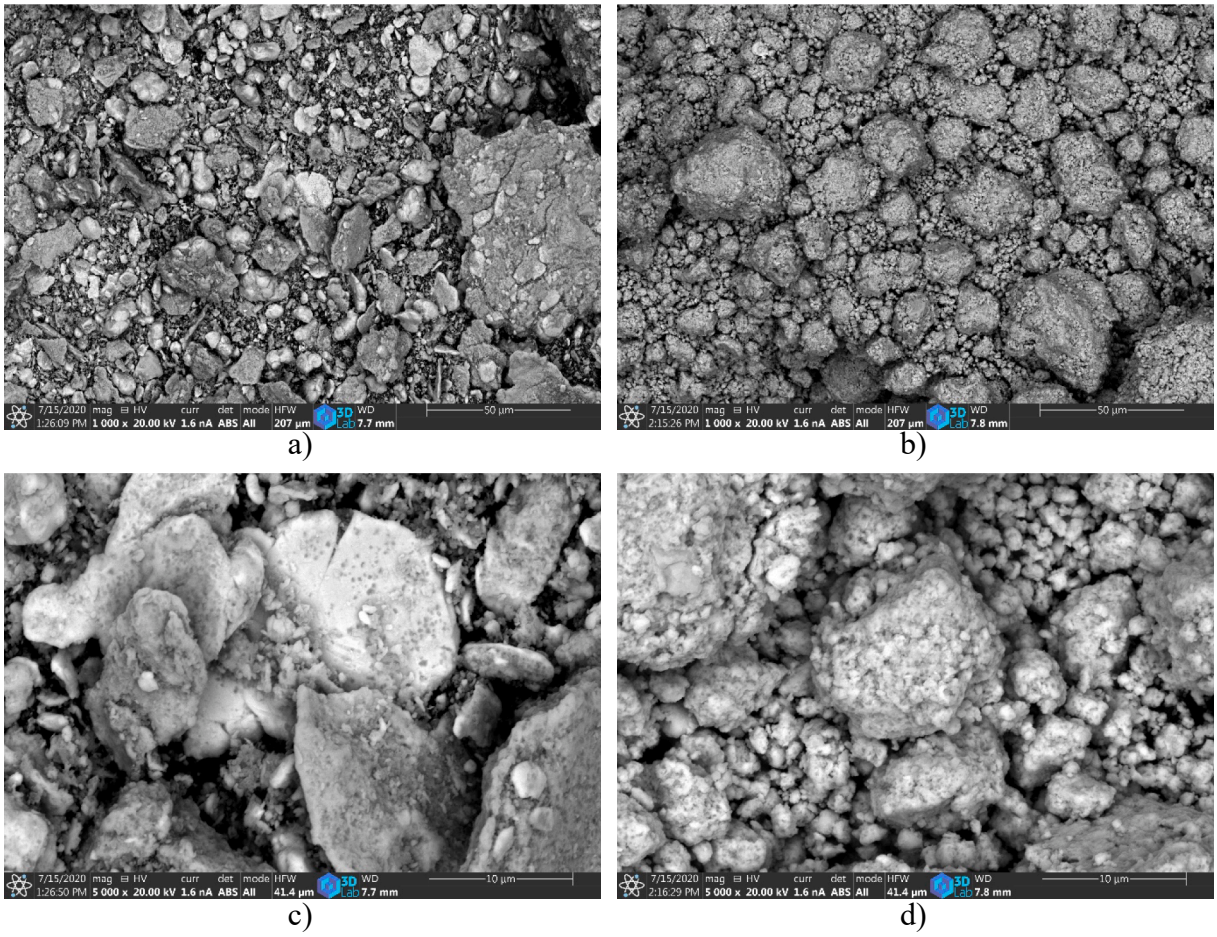

Fig. 4. SEM images with different magnifications, a-c) 2.5 BPR; b-d) 5 BPR.

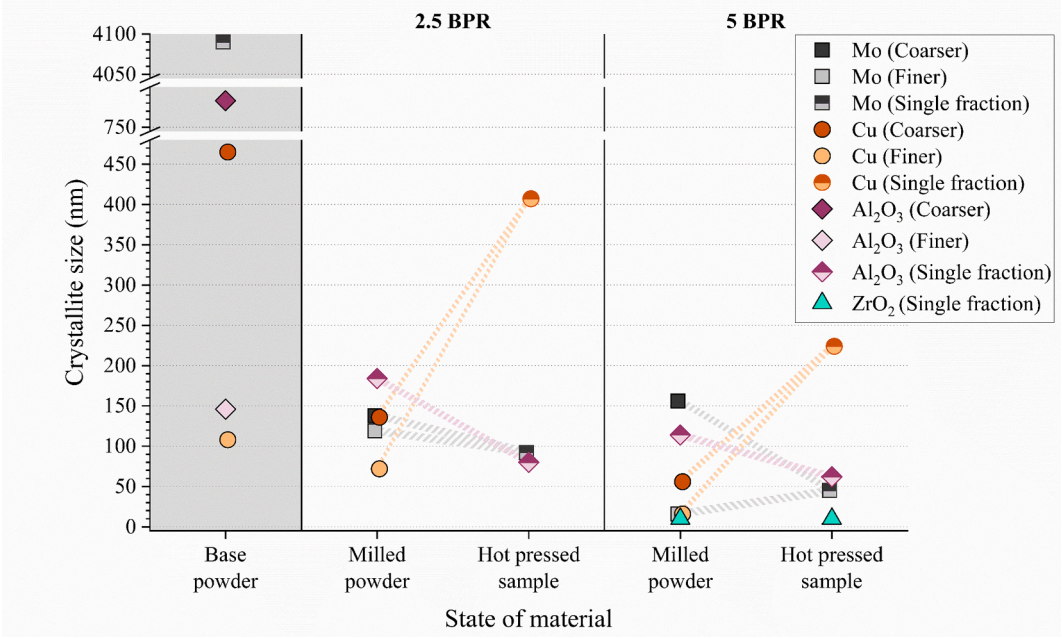

Fig. 5. Crystallite size comparison of the milled powders and hot pressed samples of 2.5 BPR and 5 BPR. The crystallite size of the base powders are also shown.

are equiaxial and the phase distribution is homogenous,but here the phases are indistinguishable from each other. In both samples the particles tend to weld together to form larger agglomerates. The evolution of particles in the Mo-Cu-Al_2O_3 composite powders, can be explained by the five stages of mechanical alloying of a ductile-brittle system [5]. Based on the images, the 2.5 BPR is in the early second stage of period of the welding predominance, having multilayered, oriented lamellae (Fig. 3c lower right corner), the 5 BPR powder has reached the third stage of equiaxed particle formation, where the aspect ratio of the formed lamellae is decreased. This happens due to the fact that the flattened, work-hardened particles are more brittle, thus get fragmented in the milling process [32].

3.2. Bulk materials

The crystallite sizes from the XRD analysis can be seen on Fig. 5. Compared to the milled powders, the size of Cu crystallites by hot pressing in both samples grew in a great extent, which indicates that recrystallization occurred at 950 °C. In the case of Mo, the hot pressing temperature is below its recrystallization temperature [41,42], so its crystallite size could not increase. The deformation during cold and hot pressing resulted in smaller crystallites within the Mo and α-Al_2O_3 as it can be seen in the case of the hot pressed 2.5 BPR sample. In the hot pressed 5 BPR sample, the crystallite size of Mo and α-Al_2O_3 was smaller, so in the case of Mo, mainly the coarse fraction decreased in crystallite size, moreover the crystallite size of ZrO_2 did not change due to deformation, since it was already around 10 nm. The decrease in α-Al_2O_3 crystallite size by hot pressing is related to the existence of cleavage planes in the crystal structure along rhombohedral direction [43] due to which it acts brittle. During the hot pressing, the heating eliminated most of the lattice strain present at the highly deformed areas in the Mo and Cu, which evened out the stresses in the respective phases throughout the specimen [44]. The subsequent cooling caused thermal stresses due to the differences in CTE [45,46] and that results in a more uniform lattice strain in the metallic phases (Fig. 6 b). These are the reasons behind the Mo and Cu in the bulk samples having only one size fraction. Additionally the thermal stresses can also cause breakage in ceramic reinforcements [45] which could contribute to the crystallite size decrease of the α-Al_2O_3 in the bulk samples.

The lattice parameters and strain of the Mo and Cu in the 2.5 BPR and 5 BPR samples can be seen on Fig. 6. There were some fractions in the powders which did not have any strain value after the Rietveld refinement, so they are not plotted.The lattice parameter value of the 2.5 BPR milled powder compared to the base powder's is only slightly different, indicating minimal deformation which is in good accordance with the morphology of the powder (Fig. 4) and by that extent, its stage in mechanical alloying. That stands also for the 5 BPR milled powder, having been on the third stage of mechanical alloying, therefore it had a slight increase in the lattice parameters. These are also in agreement with the crystallite size decrease seen on Fig. 5. The uniform lattice parameter values in both samples after hot pressing, might be caused by either oxygen diffusion along dislocation edges or as a thin oxide layer on the surface of the grains [9], which is in good agreement with literature findings [47]. This process is supported also by the absence of Mo—Cu solutions, which could be the other reason for lattice parameter change. If the formation of a Mo(Cu) or Cu(Mo) solid solution occurred, it would have increased the lattice parameter of Mo simultaneously with the decrease of Cu's lattice parameter [7], moreover it would have been detected in the milled state (Fig. 3).

The strain values in both samples (Fig. 6b) clearly were increased by milling, which were then decreased by the subsequent hot pressing. The increasement of strain values during milling is caused by vacancies, dislocations and stacking faults, as evidenced in [9]. The hot pressing carried out at 950 °C decreased the strain value in both Mo and Cu. In the case of Cu, the hot pressing temperature is quite close to its melting temperature, moreover it was in a cold-worked state, therefore recrystallization (or grain boundary migration) must have happened. This is in good agreement with its crystallite size in hot pressed state (Fig. 5). However the Mo had no increase in crystallite size in hot pressed state. Since its strain also decreased after the hot consolidation, the only possible explanation is, that Mo was annealed during hot pressing. This is also backed up by the fact that Mo is a metal with high stacking fault energy (SFE) (γ_{SFE} = 300 mJ/m^2) [48],which is much more prone to significant recovery than a metal with low stacking fault energy, such as Cu (γ_{SFE} = 78 mJ/m^2) [44]. Therefore the decrease in crystallite size due to deformation and the recovery during hot pressing are separated. The explanation behind the strain values is also backed up by the formation of single fractions in the metallic phases (Fig. 5) and by the fact that the BPR value only had a slight effect on it.

On Fig. 7. SEM images of the bulk samples made from both samples can be seen. The hot pressed 2.5 BPR consists of Mo grains (bright) surrounded by Cu grains (gray) mixed with α-Al_2O_3 (black dots). This is due to the fact that the Mo-Cu-Al_2O_3 is a ductile-brittle system during milling, hence the brittle dispersoid should be entrapped in the ductile

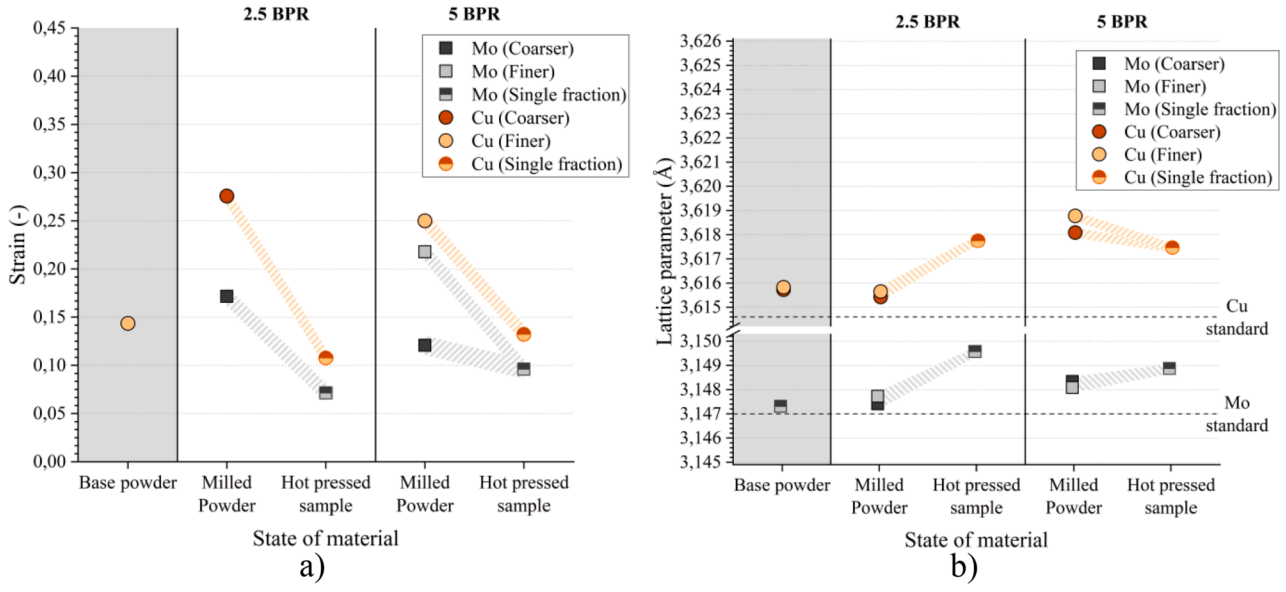

Fig. 6. Measured parameters of the milled powders and the hot pressed samples of 2.5 BPR and 5 BPR: a) Lattice parameter; b) e0. The base powders are also shown.

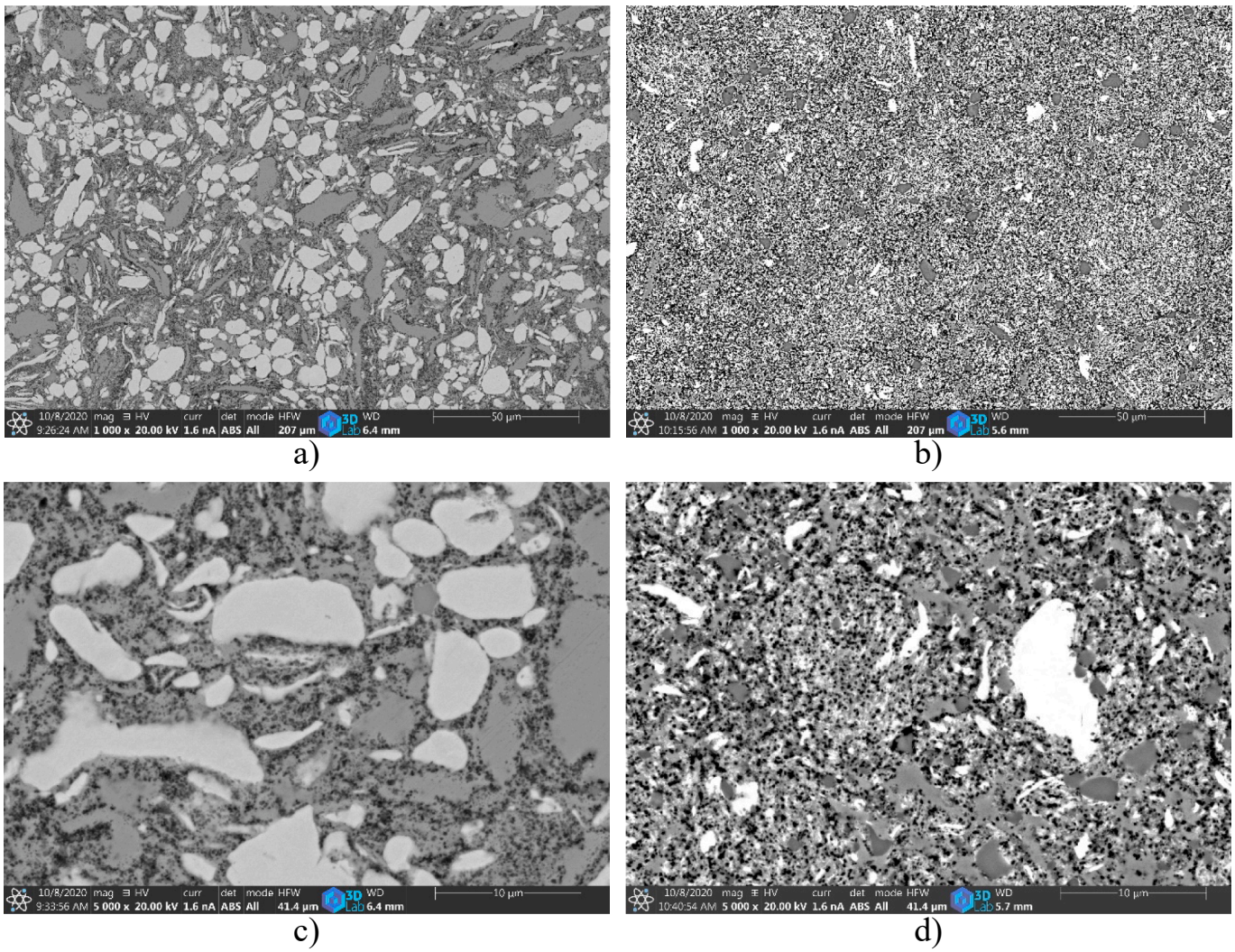

Fig. 7. SEM images of the bulk samples with different magnifications, a-c) Hot pressed 2.5 BPR; b-d) Hot pressed 5 BPR (Mo-bright, Cu-gray, Al_2O_3-black).

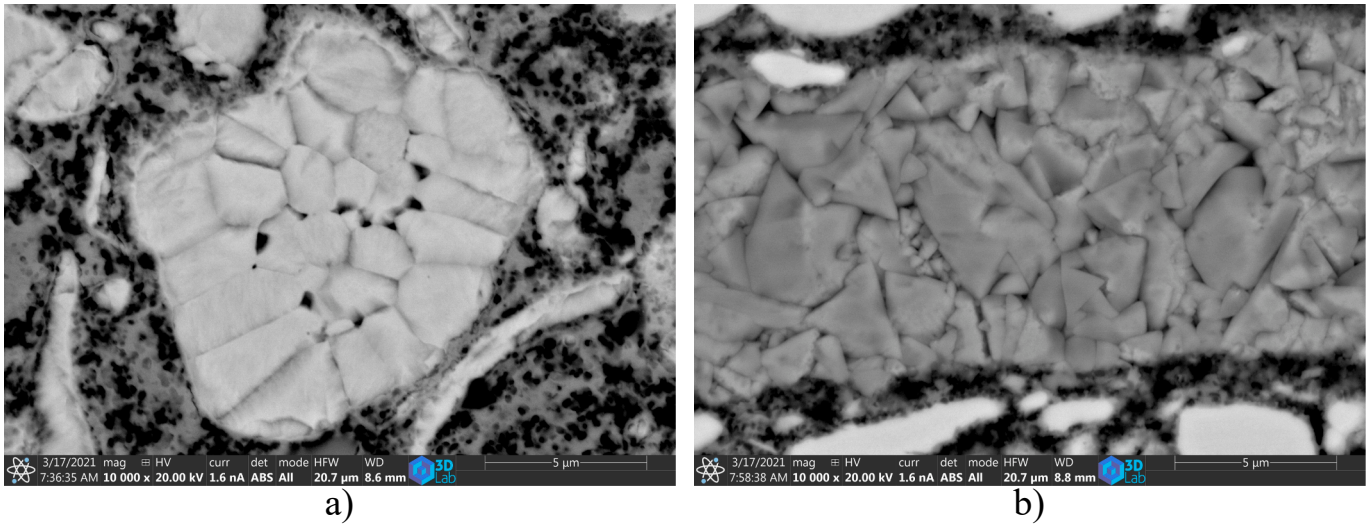

Fig. 8. SEM images of the 2.5 BPR bulk samples in 10,000 × magnification, a) etched for Mo; b) etched for Cu.

phase along the cold welded interfaces [5,32]. Since between the Mo and Cu, the Cu is the more ductile phase, α-Al_2O_3 is concentrated here. Cu grains are also prone to be elongated due to deformation by milling. In the case of 5 BPR the images show a rather fine microstructure compared to 2.5 BPR, due to the larger ball to powder ratio [6]. At lower magnification (Fig. 7b) almost no grain boundaries are distinguishable (apart from some Mo grains) and the distribution of α-Al_2O_3 is homogenous. At higher magnification it can be seen that the grains are much smaller. Also there are ZrO_2 particles (dark gray) embedded in the matrix.

To reveal the inner structure of the large grains seen in the microstructure of the bulk samples of 2.5 BPR, the samples were etched selectively for Mo and Cu as it can be seen on Fig. 8. When Mo grains welded together during milling, α-Al_2O_3 particles got trapped on the grain boundaries. The Mo and α-Al_2O_3 are clearly distinguishable within the particle. In the case of Cu, when its grains welded together and the α-Al_2O_3 got trapped inside, the ceramic reinforcement did not stay on the grain boundaries, but penetrated the grains (faint gray dots) [49,50]. This indicates that the Zener pinning effect of the α-Al_2O_3 is the reason behind, that the highly deformed Cu, at hot pressing temperature close to its melting point (1083 °C) [1], had increased only moderately in crystallite size (Fig. 5) [51]. The α-Al_2O_3 particles within the matrix can act as a nucleation site for Particle Stimulated Nucleation (PSN) [44,52], or due to the small size (around 0.1 μm) of the α-Al_2O_3 particles they could even locally inhibit recrystallization, substituting it with intensive subgrain growth [44,52,53]. Both of these mechanisms result in small, randomly oriented Cu grains within the composite resulting in the final crystallite (subgrain) sizes.

Moreover, comparing the same sized Mo and Cu particles on the image, it can be seen that the Cu particle is composed of numerous grains with a wide range of grain sizes. These are all in good accordance with the stacking fault energy of the two metals described above and their strength values. The Cu absorbs the most of the energy of the milling by forming multitude of grain boundaries and because the Mo is more resistant to deformation, it mainly acts as a reinforcement of the Cu. This is also the reason why the lattice strain of Cu in the bulk samples is higher than the lattice strain of the Mo (Fig. 6b). Furthermore, Fig. 8a) shows that Mo grains even when not welded together, stay separated from the other phases, Cu however forms a mixture with α-Al_2O_3 with no visible grain boundaries (in accordance with the crystallite size fractions shown in Table 1). Therefore in Mo—Cu pseudo-alloys reinforced with α-Al_2O_3 particles, Cu clearly is the main matrix of the ceramic reinforcement.

In Table 2. the relative density and hardness values, gained by measuring all the parallel specimens, can be seen. The relative density values indicate that the hot pressed 2.5 BPR is more easily deformable, due to its lower ceramic content and its lower strain hardening at milling. This is backed up by the hardness of the hot pressed 5 BPR which is considerably larger than the hot pressed 2.5 BPR. Both commercially available and research produced Mo—Cu alloys with 50 wt% Cu content have hardness values between 140 and 160 HB [2,8], which is significantly lower than even the hardness of the 2.5 BPR bulk sample. The increased hardness of the 2.5 BPR and 5 BPR samples can be explained by several mechanisms enhancing each other. The deformation of crystallites during milling increased the amount of crystal defects and decreased the crystallite size (Fig. 5) of the matrix, which in the next manufacturing steps resulted in higher hardness [54–56]. Moreover, the α-Al_2O_3 particles generated dislocations in the metal matrix during penetration and hindered dislocation movement in the metal lattice, contributing to the increased hardness values [55–57]. Furthermore, the hot pressing (950 °C) resulted in only a moderate crystallite size increase of copper (Fig. 5), therefore the hardness is expected to be preserved when subjected to high temperatures. Based on the results, α-Al_2O_3 particles can be used to reinforce Mo—Cu pseudo-alloys to produce a coarsening resistant nano-composite. Since one of the key features of heat sinks, apart from heat dissipation, is structural integrity [4], the increased hardness and the resistance to coarsening of the Mo—Cu based MMC, should increase the operating temperature range of these parts.

Table 2
Relative density and hardness data for the hot pressed specimens compared to the literature.

	Relative density (%)		Hardness (HB)	
	Average	Deviation	Average	Deviation
Hot pressed 2.5 BPR	97.2	0.5	286	6
Hot pressed 5 BPR	92.4	1.7	363	9
50Mo-50Cu (wt%) [2]	N/A	N/A	150 (HV)	N/A
53Mo-47Cu (wt%) [8]	99.0–99.5	N/A	140–160	N/A

4. Conclusions

The effect of different ball to powder ratios during mechanical alloying on a novel nano-crystalline material, 45Mo-45Cu-10Al_2O_3, was investigated. The milled powders and the bulk samples were analyzed by XRD, SEM and hardness measurement to evaluate the effect of BPR. The following conclusions can be made:

1) Both of the milled powders are nanocrystalline, but due to the higher ball to powder ratio, the phases in the milled 5 BPR powder had broader and lower peaks therefore lower crystallite sizes and higher strain compared to the phases in the milled 2.5 BPR powder.
2) The milling results in two separate fractions (differentiated by crystallite size and lattice distortion) in both metallic phases. Mo either forms larger particles by welding or the single grains get deformed by the milling balls. Cu particles can also weld together or get mixed with α-Al_2O_3.
3) The milled powders of 2.5 BPR and 5 BPR are in different stages of mechanical alloying, in 2.5 BPR the particles have sharp edges and are composed of large particles consisting of smaller particles welded together. However, in 5 BPR the constituents are finer, hence more evenly distributed and the particles are equiaxial.
4) In both bulk hot pressed samples the Cu had increased crystallite size, which indicates that grain boundary migration took place. Compared to the milled powder, Mo and α-Al_2O_3 has decreased its crystallite size due to deformation. The heating eliminated most of the lattice defects at the highly strained areas and the subsequent cooling resulted in uniform stresses in the respective metallic phases, thereby forming evenly distorted lattices.
5) The lattice parameter values of the bulk phases exclude the formation of Mo(Cu) and Cu(Mo) solid solutions. The lattice strain of the hot pressed samples indicate the annealing of Mo and the recrystallization of Cu (in agreement with the SFE values).
6) The microstructure of the hot pressed 2.5 BPR consists of Mo grains surrounded with the blend of Cu and α-Al_2O_3, since between the metallic phases, the Cu is the more ductile and by mechanical alloying theory, it should contain the brittle phase. In the case of 5 BPR, it has a homogenous distribution of phases, with small grains of Mo.
7) The separate etching of the metallic phases in 2.5 BPR bulk samples revealed that Mo grains welded together have the ceramic reinforcement congregated at its grain boundaries separating three or more grains. Larger Cu particles on the other hand are composed of numerous smaller grains containing α-Al_2O_3 particles which can be found within the grains. The α-Al_2O_3 particles can induce PSN or intensive subgrain growth during heating, both result in the moderate crystallite size growth of Cu.
8) The low SFE and strength of Cu explains the multitude of grains forming in the larger particles, implying that the milling causes deformation mostly in the Cu particles, also shown by the higher lattice strain values. The Mo mainly acts as a reinforcement of the composite, therefore the main matrix of the α-Al_2O_3 is the Cu.

9) Its higher ceramic content and higher deformation during milling, resulted in the 5 BPR samples having higher hardness, but lower relative density compared to 2.5 BPR bulk samples, which reached 97.2% and hardness values still significantly higher than Mo—Cu alloys. Therefore 2.5 BPR samples are a better candidate for future research and application with their higher relative density, high hardness, and interconnected Cu grains.

Declaration of Competing Interest

The authors declare that they have no known competing financial interests or personal relationships that could have appeared to influence the work reported in this paper.

Acknowledgements

The research was supported by the GINOP-2.3.2-15-2016-00027 "Sustainable operation of the workshop of excellence for the research and development of crystalline and amorphous nanostructured materials" project implemented in the framework of the Szechenyi 2020 program. The realization of this project is supported by the European Union. The authors would like to thank Dr. Dániel Koncz-Horváth for SEM measurements carried out on the samples.

References

[1] X.C. Tong, Advanced Materials for Thermal Management of Electronic Packaging vol. 30, Springer New York, New York, NY, 2011, https://doi.org/10.1007/978-1-4419-7759-5.
[2] G. Jiang, L. Diao, K. Kuang, Adv. Therm. Manag. Mater. (2013), https://doi.org/10.1007/978-1-4614-1963-1.
[3] D. Frear (Ed.), Packaging Materials BT - Springer Handbook of Electronic and Photonic Materials, Springer International Publishing, Cham, 2017, p. 1, https://doi.org/10.1007/978-3-319-48933-9_53. S. Kasap and P. Capper, Eds.
[4] C. Zweben (Ed.), Electronic Packaging: Heat Sink Materials, Elsevier, Oxford, 2001, pp. 2676–2682, https://doi.org/10.1016/B0-08-043152-6/00479-4. K. H. J. Buschow, R. W. Cahn, M. C. Flemings, B. Ilschner, E. J. Kramer, S. Mahajan, and P. B. T.-E. of M. S. and T. Veyssière, Eds.
[5] P.R. Soni, Mechanical Alloying: Fundamentals and Applications, Cambridge Int Science Publishing, 2000.
[6] M.S. El-Eskandarany, Mechanical Alloying: Nanotechnology, Materials Science and Powder Metallurgy, Elsevier, 2015.
[7] E. Botcharova, J. Freudenberger, L. Schultz, Mechanical alloying of copper with niobium and molybdenum, J. Mater. Sci. 39 (16–17) (2004) 5287–5290, https://doi.org/10.1023/B:JMSC.0000039230.73188.5d.
[8] P. Yih, D.D.L. Chung, Copper-matrix molybdenum particle composites made from copper coated molybdenum powder, J. Electron. Mater. 24 (7) (1995) 841–851, https://doi.org/10.1007/BF02653333.
[9] A. Kumar, K. Jayasankar, M. Debata, A. Mandal, Mechanical alloying and properties of immiscible Cu-20 wt.% Mo alloy, J. Alloys Compd. 647 (2015) 1040–1047, https://doi.org/10.1016/j.jallcom.2015.06.129.
[10] F. Jinglian, C. Yubo, L. Tao, T. Jiamin, Sintering behavior of nanocrystalline Mo-Cu composite powders, Rare Metal Mater. Eng. 38 (10) (2009) 1693–1697, https://doi.org/10.1016/S1875-5372(10)60051-3.
[11] D. Wang, B. Yin, A. Sun, X. Li, C. Qi, B. Duan, Fabrication of Mo–Cu composite powders by heterogeneous precipitation and the sintering properties of the composite compacts, J. Alloys Compd. 674 (2016) 347–352, https://doi.org/10.1016/j.jallcom.2016.03.027.
[12] G.A. Tikhii, N.I. Kachalin, V.P. Belova, V.I. Nikitin, Study of a Mo-Cu pseudoalloy obtained from mechanically activated charge, Met. Sci. Heat Treat. 49 (9–10) (2007) 448–452, https://doi.org/10.1007/s11041-007-0084-8.
[13] P.A. Benavides, B. Soto, R.H. Palma, Liquid phase sintering of mechanically alloyed Mo-Cu powders, Mater. Sci. Eng. A 701 (2017) 237–244, https://doi.org/10.1016/j.msea.2017.06.090.
[14] J.L. Johnson, Activated liquid phase sintering of W–Cu and Mo–Cu, Int. J. Refract. Met. Hard Mater. 53 (2015) 80–86, https://doi.org/10.1016/j.ijrmhm.2015.04.030.
[15] R. Casati, M. Vedani, Metal matrix composites reinforced by nano-particles—a review, Metals (Basel) 4 (2014) 65–83, https://doi.org/10.3390/met4010065.
[16] W.S. Barakat, A. Wagih, O.A. Elkady, A. Abu-Oqail, A. Fathy, A. EL-Nikhaily, Effect of Al2O3 nanoparticles content and compaction temperature on properties of Al–Al2O3 coated Cu nanocomposites, Compos. Part B Eng. 175 (2019) 107140, https://doi.org/10.1016/j.compositesb.2019.107140.
[17] A. Abu-Oqail, A. Wagih, A. Fathy, O. Elkady, A.M. Kabeel, Effect of high energy ball milling on strengthening of Cu-ZrO2 nanocomposites, Ceram. Int. 45 (5) (2019) 5866–5875, https://doi.org/10.1016/j.ceramint.2018.12.053.
[18] M.S. Abd-Elwahed, A.F. Meselhy, Experimental investigation on the mechanical, structural and thermal properties of Cu–ZrO2 nanocomposites hybridized by graphene nanoplatelets, Ceram. Int. 46 (7) (2020) 9198–9206, https://doi.org/10.1016/j.ceramint.2019.12.172.
[19] A.M. Sadoun, I.M.R. Najjar, M.S. Abd-Elwahed, A. Meselhy, Experimental study on properties of Al–Al2O3 nanocomposite hybridized by graphene nanosheets, J. Mater. Res. Technol. 9 (6) (2020) 14708–14717, https://doi.org/10.1016/j.jmrt.2020.10.011.
[20] A.M. Sadoun, A. Fathy, A. Abu-Oqail, H.T. Elmetwaly, A. Wagih, Structural, mechanical and tribological properties of Cu–ZrO2/GNPs hybrid nanocomposites, Ceram. Int. 46 (6) (2020) 7586–7594, https://doi.org/10.1016/j.ceramint.2019.11.258.
[21] D.Y. Ying, D.L. Zhang, Processing of Cu–Al2O3 metal matrix nanocomposite materials by using high energy ball milling, Mater. Sci. Eng. A 286 (1) (2000) 152–156, https://doi.org/10.1016/S0921-5093(00)00627-4.
[22] S.J. Hwang, J. Lee, Mechanochemical synthesis of Cu–Al2O3 nanocomposites, Mater. Sci. Eng. A 405 (1–2) (2005) 140–146, https://doi.org/10.1016/j.msea.2005.05.077.
[23] L. Xu, S. Wei, D. Zhang, Y. Li, G. Zhang, J. Li, Fine structure and interface characteristic of α-Al2O3 in molybdenum alloy, Int. J. Refract. Met. Hard Mater. 41 (2013) 483–488, https://doi.org/10.1016/j.ijrmhm.2013.06.006.
[24] Y. Zhou, Y. Gao, S. Wei, K. Pan, Y. Hu, Preparation and characterization of Mo/Al2O3 composites, Int. J. Refract. Met. Hard Mater. 54 (2016) 186–195, https://doi.org/10.1016/j.ijrmhm.2015.07.033.
[25] L. Xu, S. Wei, J. Li, G. Zhang, B. Dai, Preparation, microstructure and properties of molybdenum alloys reinforced by in-situ Al2O3 particles, Int. J. Refract. Met. Hard Mater. 30 (1) (2012) 208–212, https://doi.org/10.1016/j.ijrmhm.2011.08.012.
[26] A.M. Sadoun, M.M. Mohammed, A. Fathy, O.A. El-Kady, Effect of Al2O3 addition on hardness and wear behavior of Cu–Al2O3 electro-less coated Ag nanocomposite, J. Mater. Res. Technol. 9 (3) (2020) 5024–5033, https://doi.org/10.1016/j.jmrt.2020.03.020.
[27] A.M. Sadoun, M.M. Mohammed, E.M. Elsayed, A.F. Meselhy, O.A. El-Kady, Effect of nano Al2O3 coated Ag addition on the corrosion resistance and electrochemical behavior of Cu-Al2O3 nanocomposites, J. Mater. Res. Technol. 9 (3) (2020) 4485–4493, https://doi.org/10.1016/j.jmrt.2020.02.076.
[28] S. Morady, M. Talafi Noghani, M. Saghafi Yazdi, Effect of processing parameters on the mechano-chemical synthesis of nano crystalline Mo-Cu/Al2O3 composite, J. Ultrafine Grained Nanostruct. Mater 51 (1) (2018) 13–19, https://doi.org/10.22059/jufgnsm.2018.01.02.
[29] S. Sabooni, T. Mousavi, F. Karimzadeh, Mechanochemical assisted synthesis of Cu (Mo)/Al2O3 nanocomposite, J. Alloys Compd. 497 (1–2) (2010) 95–99, https://doi.org/10.1016/j.jallcom.2010.03.048.
[30] J. Zygmuntowicz, M. Piątek, M. Wachowski, P. Piotrkiewicz, W. Kaszuwara, Thermoanalytical and dilatometric studies of the Al2O3–Cu–Mo hybrid composite, J. Therm. Anal. Calorim. 142 (1) (2020) 51–62, https://doi.org/10.1007/s10973-020-09526-w.
[31] Z. Justyna, Ł. Agata, P. Paulina, K. Waldemar, Al2O3-Cu-Mo hybrid composites: fabrication, microstructure, properties, Compos. Theory Pract. 2 (2019) 43–49 [Online]. Available: https://www.researchgate.net/publication/338410363_Al2O3-Cu-Mo_HYBRID_COMPOSITES_FABRICATION_MICROSTRUCTURE_PROPERTIES.
[32] C. Suryanarayana, Mechanical alloying and milling, Prog. Mater. Sci. 46 (1) (2001) 1–184, https://doi.org/10.1016/S0079-6425(99)00010-9.
[33] T. Runčevski, Rietveld refinement practical powder diffraction pattern analysis using TOPAS. By Robert E. Dinnebier, Andreas Leineweber and John SO Evans. De Gruyter, 2019, J. Appl. Crystallogr. 52 (5) (2019) 1238–1239, https://doi.org/10.1107/S1600576719011178.
[34] E. Zolotoyabko, Determination of the degree of preferred orientation within the March–Dollase approach, J. Appl. Crystallogr. 42 (3) (2009) 513–518, https://doi.org/10.1107/S0021889809013727.
[35] T. Mikó, et al., Investigation of nanocrystalline sintered W-25 wt% Cu composite, Int. J. Refract. Met. Hard Mater. 95 (2021) 105438, https://doi.org/10.1016/j.ijrmhm.2020.105438.
[36] C. Aguilar, et al., Structural study of nanocrystalline solid solution of Cu–Mo obtained by mechanical alloying, Mater. Sci. Eng. A 548 (2012) 189–194, https://doi.org/10.1016/j.msea.2012.03.105.
[37] C. Suryanarayana, E. Ivanov, V.V. Boldyrev, The science and technology of mechanical alloying, Mater. Sci. Eng. A 304 (2001) 151–158, https://doi.org/10.1016/S0921-5093(00)01465-9.
[38] Y. Saberi, S.M. Zebarjad, G.H. Akbari, On the role of nano-size SiC on lattice strain and grain size of Al/SiC nanocomposite, J. Alloys Compd. 484 (1–2) (2009) 637–640, https://doi.org/10.1016/j.jallcom.2009.05.009.
[39] W. Qin, J.A. Szpunar, Origin of lattice strain in nanocrystalline materials, Philos. Mag. Lett. 85 (12) (2005) 649–656, https://doi.org/10.1080/09500830500474339.
[40] D.W.A. Rees, Deformation and fracture of metal matrix particulate composites under combined loadings, Compos. A Appl. Sci. Manuf. 29 (1) (1998) 171–182, https://doi.org/10.1016/S1359-835X(97)00050-X.
[41] T. Mrotzek, A. Hoffmann, U. Martin, Hardening mechanisms and recrystallization behaviour of several molybdenum alloys, Int. J. Refract. Met. Hard Mater. 24 (4) (2006) 298–305, https://doi.org/10.1016/j.ijrmhm.2005.10.003.
[42] S. Primig, H. Leitner, H. Clemens, A. Lorich, W. Knabl, R. Stickler, On the recrystallization behavior of technically pure molybdenum, Int. J. Refract. Met. Hard Mater. 28 (6) (2010) 703–708, https://doi.org/10.1016/j.ijrmhm.2010.03.006.
[43] H.S. Bagdasarov, G.V. Berezhkova, V.G. Govorkov, E.P. Kozlovskaya, E.A. Fedorov, M.A. Chernysheva, The geometry of fractures caused by cleavage of α-Al2O3 single

crystals, Krist. Tech. 8 (4) (1973) 507–511, https://doi.org/10.1002/crat.19730080414.
[44] F.J. Humphreys, M. Hatherly, Recrystallization and Related Annealing Phenomena, Elsevier, 2012.
[45] K.K. Chawla, Metal matrix composites, in: Composite Materials, Springer, 2012, pp. 197–248, https://doi.org/10.1007/978-0-387-74365-3_6.
[46] A. Sanaty-Zadeh, Comparison between current models for the strength of particulate-reinforced metal matrix nanocomposites with emphasis on consideration of Hall–Petch effect, Mater. Sci. Eng. A 531 (2012) 112–118, https://doi.org/10.1016/j.msea.2011.10.043.
[47] M. Efe, H.J. Kim, S. Chandrasekar, K.P. Trumble, The chemical state and control of oxygen in powder metallurgy tantalum, Mater. Sci. Eng. A 544 (2012) 1–9, https://doi.org/10.1016/j.msea.2012.01.100.
[48] L.M. Voronova, T.I. Chashchukhina, T.M. Gapontseva, Y.G. Krasnoperova, M. V. Degtyarev, V.P. Pilyugin, Effect of the deformation temperature on the structural refinement of BCC metals with a high stacking fault energy during high pressure torsion, Russ. Metall. 2016 (10) (2016) 960–965, https://doi.org/10.1134/S0036029516100232.
[49] P.K. Jena, E.A. Brocchi, M.S. Motta, In-situ formation of Cu–Al2O3 nano-scale composites by chemical routes and studies on their microstructures, Mater. Sci. Eng. A 313 (1–2) (2001) 180–186, https://doi.org/10.1016/S0921-5093(00)01998-5.
[50] M.S. Motta, P.K. Jena, E.A. Brocchi, I.G. Solorzano, Characterization of Cu–Al2O3 nano-scale composites synthesized by in situ reduction, Mater. Sci. Eng. C 15 (1–2) (2001) 175–177, https://doi.org/10.1016/S0928-4931(01)00272-7.
[51] S.B. Chandrasekhar, S.S. Sarma, M. Ramakrishna, P.S. Babu, T.N. Rao, B. P. Kashyap, Microstructure and properties of hot extruded Cu–1 wt% Al2O3 nano-composites synthesized by various techniques, Mater. Sci. Eng. A 591 (2014) 46–53, https://doi.org/10.1016/j.msea.2013.10.074.
[52] J.E. Allison, J.W. Jones, S. Suresh, A. Mortensen, A. Needleman, in: S. Suresh, A. Mortensen, A. Needleman (Eds.), Fundamentals of metal matrix composites, Butterworth-Heinemann, 1993.
[53] T.W. Clyne, P.J. Withers, An Introduction to Metal Matrix Composites, Cambridge University Press, 1995.
[54] M. Shaat, A. Fathy, A. Wagih, Correlation between grain boundary evolution and mechanical properties of ultrafine-grained metals, Mech. Mater. 143 (2020) 103321, https://doi.org/10.1016/j.mechmat.2020.103321.
[55] A.I. Khdair, A. Fathy, Enhanced strength and ductility of Al-SiC nanocomposites synthesized by accumulative roll bonding, J. Mater. Res. Technol. 9 (1) (2020) 478–489, https://doi.org/10.1016/j.jmrt.2019.10.077.
[56] A. Wagih, A. Fathy, D. Ibrahim, O. Elkady, M. Hassan, Experimental investigation on strengthening mechanisms in Al-SiC nanocomposites and 3D FE simulation of Vickers indentation, J. Alloys Compd. 752 (2018) 137–147, https://doi.org/10.1016/j.jallcom.2018.04.167.
[57] M.S. Abd-Elwahed, A.F. Ibrahim, M.M. Reda, Effects of ZrO2 nanoparticle content on microstructure and wear behavior of titanium matrix composite, J. Mater. Res. Technol. 9 (4) (2020) 8528–8534, https://doi.org/10.1016/j.jmrt.2020.05.021.